WIDE COVERAGE, FINE RESOLUTION, GEOSYNCHRONOUS SAR FOR ATMOSPHERE AND TERRAIN OBSERVATIONS

A Monti Guarnieri[(1)], F. Djelaili[(2)], D. Schulz[(2)], V. T. Khang[(2)], A. Recchia[(1)], F. Rocca[(1)], D. Giudici[(3)], S. Hobbs[(4)], T. Strozzi[(5)], C. Werner[(5)], R. Venturini[(6)], A. Broquetas[(7)], J. Ruiz-Rodon[(7)], G. Wadge [(8)]

[(1)] DEIB-Politecnico di Milano, Piazza Leonardo da Vinci, 32 – 20133 Milano. Email: monti@elet.polimi.it
[(2)] SES, [(2)] Aresys, [(3)]Gamma Remote Sensing, [(4)] Cranfield University, [(5)] Thales Alenia Space Italy, [(6)] Universitat Politècnica de Catalunya, [(7)] Meteorology, University of Reading

ABSTRACT

The paper proposes a COMmunication SATellite (COMSAT) compatible Synthetic Aperture RADAR (SAR), with *regional* coverage and continuous observations. Such a system could provide deformations and water-vapour maps over regions of hundreds of kilometers with resolutions in time-space otherwise impossible with that coverage. The basic monostatic concept is reviewed together with its multistatic evolution, capable of exploiting the present clusters of COMSATs at the same longitudinal node. Attention is brought to the most critical issues, such as atmospheric turbulence, target coherence, and clutter decorrelation.

1. GEO-SAR concepts

The exploitation of the eccentricity in a geosynchronous orbit for providing a synthetic aperture was proposed the first time by Kiyo Tomiyasu in '78 [1]: the system – that we may define "continental" by its coverage, exploited an inclination > 50^0 and a significant eccentricity to get the huge figure eight orbit shown in Fig. 1 on the left. Each target is observed once each day for an interval of tens of seconds to minutes, and the range swath depth can be thousands of km. Such continental coverage is achieved at the price of large antennas (7 - 30 m) and powers up to 30 kW, technologies that were defined ready for 2020 in [2].
On the other hand, the "*regional*" GEO-SAR concept we address here compensates the spread-losses thanks to the typical 42000 km range by integrating over aperture times from minutes to hours. That system, first introduced in '95[3], is quite different from the previous one as it exploits the tiny eccentricity and virtual zero inclination of COMSAT satellites, that leaves some 70 km synthetic aperture, as shown in Fig. 1. The result is that the system is continuously observing the same region on the earth, thus enabling monitoring of deformations and atmospheric turbulences [4], not achieved with the continental coverage system. Further, the major advantage of such system is to be fully compatible with a COMSAT in orbit, coverage, power and antenna requirements, and then suited to be hosted as a payload. Finally, it could even exploit digital signals, like TV broadcasts, as opportunity signals [5].

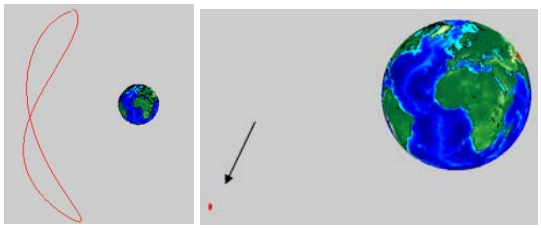

Figure 1. Geosynchronous orbits: the one for continental coverage (left) and the typical COMSAT for regional observations (right).

2. Technologies and applications

A SAR system is capable of all-weather observations, penetrates a vegetation canopy if a proper wavelength is chosen, like L-band, and can achieve millimetric accuracy in the estimation of subsidences [6].

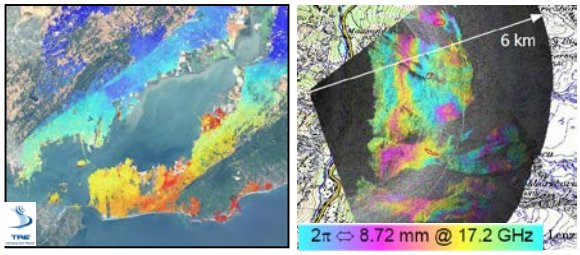

Figure 2. Typical GEO-SAR products: left, deformation map; right, atmospheric phase screen (in 18 minutes).

However, the long integration time, minutes, would prevent the observation of moving targets like water, leaves, and maybe grass, that will be cancelled out just in the ~1 s range focusing. The system would observe all the targets coherent from minutes on, like Permanent Scatterers (PS), urban areas, rocks, deserts, soil and vegetation (branches and trunks), depending on the wavelength.

A GEO-SAR system could be applied to those phenomena currently exploited by the LEO SARs (e.g. Sentinel-1), such as earthquakes, volcanic eruptions,

Proc. 'ESA Living Planet Symposium 2013', Edinburgh, UK
9–13 September 2013 (ESA SP-722, December 2013)

landslides and subsidence. However, it is the observing capabilities that are unique to GEO-SAR that are most valuable. These are:

- sub-daily imaging of phase and coherence
- continuous fast motion measurement (>cm/day)
- north-south motion sensitivity
- atmospheric phase delay maps
- column water vapour fields

Hence potentially hazardous geophysical phenomena that are preceded by accelerating motion such as landslides [7] and glaciers could be tracked and alerts flagged. Earthquake urban damage assessment [8] requires sub-daily imaging immediately post-event and decorrelation maps from GEO-SAR could supply that. Complex patterns of surface deformation during volcano deformation lasting many hours are aliased by LEO SARs [9,10] but should be accessible to GEO-SAR. Similarly, the rapid creep deformation that often follows hours to days after major earthquake ruptures is usually missed by InSAR. The availability of independent maps of phase delays due to variable atmospheric refraction that can be used to mitigate their effects on interferograms is a big prize [11].
Table 1 lists a few of the more obvious potential applications of GEO-SAR data. Not all may be fully realized, but others undoubtedly will take their place.

FIELD	APPLICATIONS	REQUIREMENTS
Earthquakes	Immediate response	High. res. coherence
	Early post-seismic	Low res. hourly diff. phase
	Improved 3D motion	N-S LOS, high res. diff. phase
Volcanic eruption	Intra-eruption deformation	Sub-daily diff. phase
	Lava flow tracking	Sub-daily coherence
Landslides	Regional triggers	High res. daily coherence
	Fast motion alert	High res. sub-daily phase
Glaciers	Fast motion alert	High res. sub-daily phase
InSAR	Water vapour correction	Low res. ~hourly phase
Meteorology	Assimilation in storm models	Low res. ~ hourly ZWD

Table 1. Some GEO-SAR applications and technical requirements

One of the major products would be the generation of water vapour maps, enabled by the capability of GEO-SAR to sense Atmospheric Phase Screens, like the one in Fig. 2 on the right, achieved by a ground-based radar within just 18 minutes of observations in Ku band. Besides these applications, there might be other ones relying on short revisit, global coverage, not yet known.

In reference [4], a dual frequency, L+Ku, system was introduced. Such a system would combine the high resolution, high sensitivity to displacements and to backscatter from point targets (like the users TVSAT parabolas) of Ku, with the unique properties of L band like penetration, good coherence, robustness versus the atmospheric turbulence. The footprint achieved by such systems are shown in Fig. 3 in the case a single reflector of 4.7 m diameter is exploited, illuminated by Ku and L-band feeders. The beams could then be pointed in different areas of interest by moving the reflector. Notice that the L-band beam would be so large (3200 km) as to cover all Europe even if the reflector pointing in significantly changed.

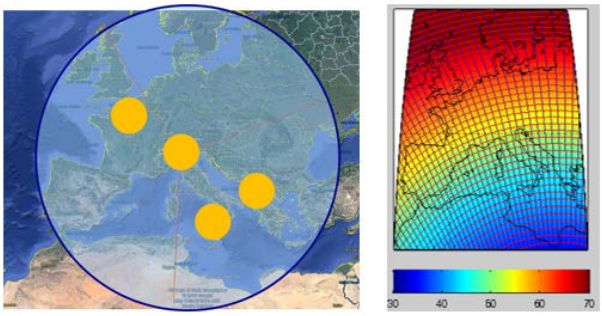

Figure 3. Left: GEO-SAR beams: high resolution (orange), Ku band, and coarse resolution (blue), L band. Right incidence angles as from 28^0 COMSAT.

The incidence angles are represented in the same figure on the right, by assuming illumination from a COMSAT placed at 28^0 E. Incidence angles in Europe vary in the range between 40^0 (south Italy), to 70^0 for Norway, so that coverage at north would be much limited by shadowing. Performances in L and Ku band are summarized in Tab. 2 for a target located at the scene centre, by assuming an orbit eccentricity of 4×10^{-4}. Notice that the final resolution, with four looks, is 100×100 m in L band and 10×10 m in Ku, but quick looks of 1 km × 100 m (L band) and 75 m × 10 m could be generated each 30'. The overall transmitted power would be 300W on the average, that is a small fraction of the future COMSAT capabilities.

3. Clutter and atmospheric decorrelation

The echo collected by a GEO-SAR upon transmission of each pulse, and then range focused, is the result of backscatter over a large area, spanning the whole antenna footprint in azimuth, shown in Fig. 3. After focusing, the energy backscattered by each target is located in the proper azimuth. However, SAR focusing is a coherent process that requires the precise knowledge of the sensor-target distance, to an accuracy comparable with the wavelength. Therefore, random changes in that distances, like due to the propagation delay in the atmosphere or the fast motion of the targets like water, grass, leaves, contribute with a phase error that may prevent focusing and, in the worst case, would

scatter energy along the whole iso-range line in the focused image.

3.1. Atmospheric Phase Screen

	L band	Ku band
Swath width	3200 km	250 km
Single look resolution: az x rg	100 m × 20 m	10 m × 2.5 m
Synthetic aperture time	5.5 hours	4 hours
S.l. resolution in 30° : az x rg	1 km × 20 m	75 m × 2.5 m
APS compensation	Not critcal	Demanding
Mean power for 0 dB SNR - distributed target, 4.7 m reflector	250 W	45 W
SNR – 80 cm user parabola	-7.8 dB	28 dB
Scene decorrelation	days	Minutes (but for urban, rocks, desert and PS)
Penetration	good	none

Table 2. GEO-SAR performances in L and Ku band.

The propagation delay has been modelled in [4] as a Normal process, by an extension of Kolmogorov turbulence [14]:

$$\Delta\phi_{aps}(t,x) \sim N\left(0, \sigma^2_{aps}(t,x)\right)$$
$$\sigma^2_{aps}(t,x) = \left(\frac{4\pi}{\lambda}\right)^2 \left(\sqrt{\left(\frac{t}{t_0}\right)^2 + \left(\frac{|x|}{x_0}\right)^2} \right) \quad (1)$$

t,x being range time and azimuth. The impact is severe at small wavelengths, λ in (1), where the phase noise, whose power is proportional to λ^{-2}, is not compensated by the linear reduction of integration time with wavelength. The time and space constant that rules the noise, t_0 and x_0 in (1), depends much upon the propagation statistics, that are not so easy to measure. Currently, Ground based RADAR (GBR) [15], GNSS [17] and meteorological models (ECWMF) can do that, with the required accuracy and coverage in time and space – but with limited accuracy in time. However, measures in time domain are much easier to get, and there is a co nsistent literature addressing both the impact on APS on GEO-SAR [13], [16], and a focusing schemes to compensate for it [18]. The APS would probably introduce too much decorrelation in Ku band to make the data useful, whereas in L band it will be much mitigated [16]. Therefore, we would exploit the L-band to estimate the APS in order to compensate most of it in the Ku band beam. L band would also allow for retrieving the **ionospheric** phase contribution, that in turns is quite relevant to compensate GPS and LEO SAR's in P, L band, as well as for scientific applications, like a possible search for earthquake precursors [19].

3.2. Clutter decorrelation

Targets that move in the antenna aperture cause clutter noise – a fact acknowledged by the very first reference for GEO-SAR [5], that significantly affects the total Signal-to-Noise-Ratio, and then impacts system design.
If we approximate GEO-SAR motion as linear, with velocity *v*, a fixed target on the scene contributes with a Doppler:

$$f_D = -\frac{2v}{\lambda}\sin\psi \approx -\frac{2v}{\lambda}\psi, \quad (2)$$

that is one-to-one related to the azimuth angle spanned from broadside, ψ. The whole scene will then be observed by an angular interval:

$$\Delta\psi = \lambda / L_a, \quad (3)$$

L_a being the real antenna length. If we define ρ_a to be the wanted resolution, the maximum antenna length would be $L_{amax}=2\,\rho_a$, and then the minimal Doppler bandwidth compatible with the resolution is, from (2):

$$B_{D\min} = \frac{2v}{L_{a\max}} = \frac{2v}{2\rho_a} = \frac{v}{\rho_a} \quad (4)$$

GEO-SAR, similarly to airborne SAR, and differently from LEO-SAR, exploits antennas much smaller than L_{amax}, and then data should be pre-summed in the Doppler bandwidth (3) to attain the acceptable Signal-To-Noise ratio. By filtering raw data, any contribution from targets moving faster than

$$v_{\max} = \frac{B_{D\min}\lambda}{2} \quad (5)$$

will vanish from the image and appear black. This does not mean that slower targets are correctly imaged. In fact, they should move say by less than a half a wavelength for an interval larger than the synthetic time, T_s (tens of minutes to hours, depending on the resolution), to get them properly focused:

$$v_{\min} = \frac{1}{4\lambda T_s} \quad (6)$$

For a linear motion, the broadening of the focused impulse response would be inversely proportional to the synthetic aperture time. Therefore, the fast moving targets, yet with velocity lower than v_{max} in (5), are those spreading energy over wider areas, as shown in Fig. 4 for leaves, in the very short integration time of an airborne data, but Ka band.

System	B_{Dmin}	T_S	Vmin	Vmax
	Hz	s	m/s	m/s
LEO-SAR	134	0.3	0.21	16.75
GEO-C	3	630	9.87E-05	0.38
GEO-R	0.05	38000	1.64E-06	0.006

Table 3. Critical targets velocities causing decorrelated clutter at L band, for 50 m resolution.

The range of "critical" velocities, $V_{min}<v<V_{max}$, is shown in Tab. 3 for LEO-SAR,as well as the continental and regional geosynchronous SAR, by assuming a 50 m resolution and L band.

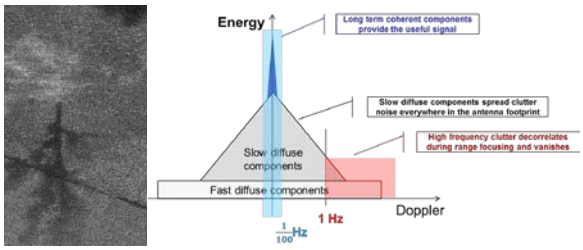

Figure 4. Left: defocusing of leaves, and scattering of clutter along azimuth, due to motion in Ka band - airborne data from [20]. Right: the Billingsley Intrinsic Clutter Motion (ICM) model 0.

The proper evaluation of the clutter impact needs a knowledge of the energy distribution with respect to velocity, that is the corresponding Doppler. This information is provided by the Billingsley ICM model, 0, that is widely used in RADAR analyses for moving targets. The model, represented in Fig. 4 on the right, comprises three regions: a DC component, corresponding to the long term stable contribution, a wideband white term, that would be mostly cancelled in presumming, and a triangular (in log-scale) component due to slow decorrelation, say Brownian model, part of which will be responsible of clutter noise. Billingsley used the NWRT RADAR to measure power spectra from VHF to W band and different vegetation and wind condition. However, this in the range from sub-Hz to tens of Hz, whereas the range of interest for GEO-SAR, both regional and continental starts from frequencies even lower than 1/100 Hz as shown in Tab. 3 and Fig. 4.

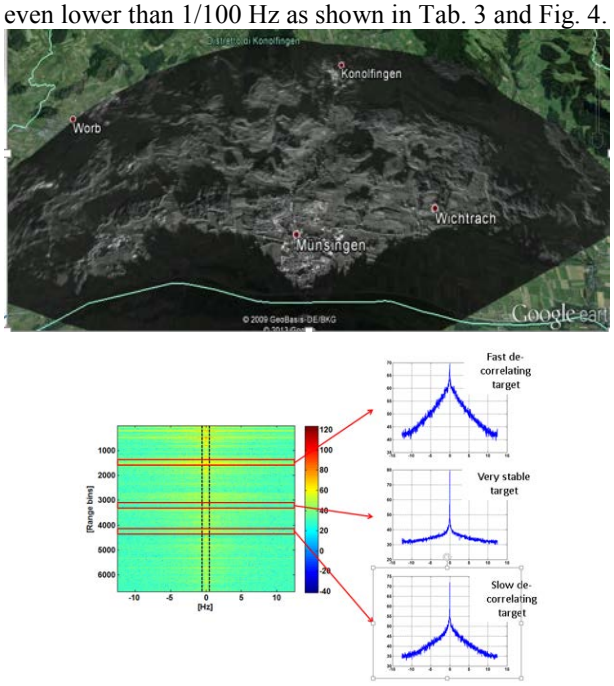

Figure 5. Preliminary measures of clutter power spectra from Ground Based RADAR. Above: RADAR detected power, superposed to Google earth (area near Bern). Below left: right power versus frequency (horizontal axis) for different range (vertical). Right: estimates of power spectra, confirming Billingsley model.

In order to assess the performance of clutter in long term, and different conditions of wind, seasons, scenes, a campaign is on-going that exploits the real aperture GB Radar of GAMMA Remote Sensing A.G.. Preliminary results, shown in Fig. 5, confirm the fitness of the model to ICM, for three targets at different range.

4. The multistatic constellation

Let us consider now a cluster of M geosynchronous satellites, like the one in Fig. 4, each located within a say 0.1° × 0.1°, 70 × 70 km, apparent square, distant R=42000 km from the target. Let us then consider a coordinate system that has its origin on the centre of the cluster, one axis z directed along the line of sight, and another axis x parallel to the isochron on the earth surface (the local parallel, in this case). Suppose that each satellite transmits at frequency $f_0+\Delta_n$ and all the n=1:N others receive. If the scene was stationary, after some time all of the target wavenumbers would be illuminated and the target spectrum would be completely recovered, typically, in a time interval say of $12/M^2$ hours. For say M = 10, this time could be as small as 7 minutes, and therefore a new image could be obtained in this very short time interval. At any given time, we remember that the k_x axis is sampled M^2 times, and the positions of the samples on that axis are random and randomly changing.

We abandon now, for simplicity, the continuum space axis for a d iscrete one, sampled at a space intervals equal to the spatial resolution δ. Indicating with Λ the width of the area illuminated on the ground, the number of samples of the sampled x a xis and therefore of the sampled k axis is

$$N = \frac{\Lambda}{\delta}$$

The random sampling of the k_x axis entails a convolution, in space, of the autocorrelation of the data with the transform of the autocorrelation of the time varying random sampling lattice. H owever, the ever changing landscape creates two different disturbing effects: atmospheric phase screen and clutter. The APS would not be a problem in the case of the constellation, even if we exploit the Ka band, thanks to the very short revisit time. Concerning clutter, let us call r the probability of hitting a sample in the k_x domain; we have

$$r = \frac{M^2}{N} << 1$$

The autocorrelation of a function that has M^2 unit spikes located at random among N positions is a spike of amplitude r in the origin plus a constant of amplitude r^2:

$$E\left[x_k^2\right] = r;\ E\left[x_k x_h\right] = r^2;\ h,k = -N/2\ :\ N/2$$

The antitransform of this acf, that we call q(n); n=1:N, is thus a function of the spatial position along the

isochrone. It is again the sum of a spike in the origin plus a constant, and the ratio of the two is 1/M². Hence, the effect of random sampling of the k_x axis is equivalent to add to the data the reflectivity **at that time** of all the neighbouring points, weighted times 1/M². Now, the stationary part of the scene will be built up as said in the time 12×3600/M² , but the changing clutter will remain as uncanceled noise on the image. True enough, this noise has zero mean, and it will disappear after a while, provided that the signal scene was meanwhile stationary.

A new independent set of values will be summed to the data as soon as the new sampling pattern becomes independent from the previous one, i.e. every τ seconds. The time τ can be evaluated as the time it takes to any sample in the k domain to move from one sampled k value to the neighbouring one, distant

$$\Delta k = \frac{2\pi}{\Lambda}$$

and thus approximately $\tau = 8*3600/N$. As N could be easily as high as 10^4, the order of magnitude for τ is thus a few seconds. So, the effects of the clutter will fast decrease with time, depending on the scene. Fast changing clutter will also be rejected, as its Doppler lays outside the visible Doppler range, so that only a reduced interval of clutter time constants will be of disturbance.

This short section was intended to show that clusters of COMSAT's could lead to *continuous* observation systems with *short* observation times, in a situation closer to a " real antenna" rather than to a "synthetic antenna". It might be possible to combine the advantages of [1] and [5], with quite lower costs.

5. Acknowledgments

The authors would like to thank ESA – ESTEC for sponsoring of the activities here described (section 3), in the frame of the project “Study on Utilisation of Future Telecom Satellites for Earth Observation”.

Figure 4. Left: SES constellation of COMSATs at 19.2^0 E, right: examples of ground tracks of orbits.

6. Conclusions

A technically innovative and observationally unique system has been described. The system is capable of providing:

- ✓ complementarity to LEO DInSAR applications
- ✓ applications involving RADAR observations in short time, medium resolution, so far achievable only by ground based UAV SAR's, but continuously and at sub-continental scale
- ✓ tropospheric and ionospheric screen maps, to be used for used for numerical weather forecast, for compensation of the atmospheric phase screen in other LEO-SAR and GPS, and for other scientific applications
- ✓ further applications involving such a continuous revisit yet to be discovered.

The system is suited to be hosted as a payload on a COMSAT, being compatible with the small eccentricity and requiring power less than 1 kW and antenna reflectors less than 5 m, then ensuring continuity of observations for the typical 15 years lifetime of COMSATs.

Finally, it could evolve in a constellation, where each payload could exploits all the IP and TV broadcasts in Ka-band as sources of opportunity achieving the full resolution, say of 3 m in azimuth, in a time interval the order of say a few minutes. Such a very short revisit time would definitely clear any issue like atmospheric phase screen or clutter decorrelation.

7. REFERENCES

[1] K.Tomiyasu, *Synthetic aperture radar in geosynchronous orbit*. IEEE Antennas and Propagation Symp., U.Maryland, pp.42-45, May 1978.

[2] W. N. Edelstein; S. N. Madsen ; A. Moussessian, C. Chen "Concepts and technologies for synthetic aperture radar from MEO and geosynchronous orbits", Proc. SPIE 5659, Jan. 18, 2005, doi:10.1117/12.578989

[3] A. Monti Guarnieri, C. Prati, F.Rocca, Frequent observation of surface motions using ScanSAR and GeoSAR, Proc. Space Congress, (Bremen, Germany), 23 May 1995, vol SAR Inteferometry, pp.61–74

[4] Andrea Monti Guarnieri, et. al. “Design of a geosynchronous SAR system for water-vapour maps and deformation estimation in proc FRINGE 2011 (Frascati, Italy) , 19-23 Sept 2011, pp 1-5.

[5] C. Prati, F. Rocca, D. Giancola, A. Monti Guarnieri. “Passive geosynchronous SAR system reusing backscattered digital audio broadcasting signals”. IEEE Trans. GRS, 36(6):1973-1976, 1998

[6] A Rucci, et. al, “Sentinel 1 SAR interferometry applications: The outlook for sub millimeter measurements”, Remote Sensing of Environment, vol 120, june, 2012, pp.156-16, Elsevier.

[7] Corsini, A., Farina, P., Antonello, G., Barbieri, M., Casagli, N., Coren, F., Guerri, L., Ronchetti, L., Sterzai, P., Tarchi, D. (2006). Space-borne and ground-based SAR interferometry as tools for landslide hazard management in civil protection. International Journal of Remote Sensing, 27 (12), 2351 - 2369.

[8] Brunner D., Lemoine, G., Bruzzone, L. “Earthquake damage assessment of buildings using VHR optical and SAR imagery” IEEE Trans. Geosc. Rem. Sens., 48, 2403-2420, 2010
[9] Lundgren P., Rosen, P.A., “Source model for the 2001 flank eruption of Mt. Etna volcano.” Geophys. Res. Lett. 30/7, 1388, 2003.
[10] Accocella, V., Neri, M., “What makes flank eruptions? The 2001 E tna eruption and its possible triggering mechanisms”, Bull. Volcano 65,517-529, 2003.
[11] Ding, X., Li, Z., Zhu, J., Feng, G., Long, J. “Atmospheric effects on InSAR measurements and their mitigation” Sensors, 8, 5426-5448, 2008.
[12] Porcello L.J., "Turbulence-Induced Phase Errors in Synthetic-Aperture Radars", *IEEE Transactions on Aerospace and Electronic Systems*, Vol. AES-6, Issue 5, pp. 636 – 644, 1970
[13] Bruno, D.; Hobbs, S.E., "Radar Imaging From Geosynchronous Orbit: Temporal Decorrelation Aspects," IEEE Trans. GRS, vol.48, no.7, pp.2924,2929, July 2010
[14] Treuhaft, R.N., Lanyi, G.E., The effect of the dynamic wet troposphere on radio interferometric measurements. Radio Science, 22(2), 251-265, 1987.
[15] Iannini, L.; Guarnieri, A.M., "Atmospheric Phase Screen in Ground-Based Radar: Statistics and Compensation," Geoscience and Remote Sensing Letters, IEEE , vol.8, no.3, pp.537,541, May 2011
[16] Kou, L.; Xiang, M.; Wang, X.; Zhu, M., "Tropospheric effects on L-band geosynchronous circular SAR imaging," Radar, Sonar & Navigation, IET , vol.7, no.6, pp.,, July 2013
[17] Realini, E., Tsuda, Toshitake, Sato, Kazutoshi, Oigwa, Masanori, Iwaki, Yuya, "Analysis of the Temporal and Spatial Variability of the Wet Troposphere at a Local Scale by High-rate PPP Using a Dense GNSS Network," Proceedings of the 25th International Technical Meeting of The Satellite Division of the Institute of Navigation (ION GNSS 2012), Nashville, TN, September 2012, pp. 3406-3412
[18] Ruiz Rodon, J.; Broquetas, A.; Monti Guarnieri, A.; Rocca, F., "Geosynchronous SAR Focusing With Atmospheric Phase Screen Retrieval and Compensation," IEEE Trans. GRS, vol.51, no.8, pp.4397,4404, Aug. 201
[19] N. Jakowski, V. Wilken, K. Tsybulya, S. Heise, Earthquake Signatures in the Ionosphere Deduced from Ground and Space Based GPS Measurements, Observation of the Earth System from Space
[20] A portfolio of fine resolution. Ka-band SAR ima ges: part I. A.W. Doerry, D.F. Dubbert,. M.E. Thompson, V.D. Gutierrez. Sandia National Laboratories
[21] J. B. Billingsley, J. F. Larrabee, Measured spectral extent of l- and x-radar reflections from windblown trees, Tech. rep., MIT Lincoln Laboratory, DTIC AD-A179942 (feb 1987)